2016

Tunable External Cavity Ring Laser with Wavelength Selective Elements

Zhi Han
Iowa State University

Tunable external cavity ring laser with wavelength selective elements

by

Zhi Han

A thesis submitted to the graduate faculty

in partial fulfillment of the requirements for the degree of

MASTER OF SCIENCE

Major: Electrical Engineering

Program of Study Committee:
Meng Lu, Major Professor
Santosh Pandey
Liang Dong

Iowa State University

Ames, Iowa

2016

TABLE OF CONTENTS

LIST OF FIGURES

ACKNOWLEDGEMENTS

I would first like to express my sincere gratitude to my major professor Meng Lu for his patience, motivation and continuous guidance through the past two years of my graduate study. Professor Meng Lu inspired me to think critically and creatively. I value the several discussions I had with him about research, thesis and most importantly in finding my future career direction. I could not have imagined having a better mentor for my graduate study. I would also like to thank my program of study committee members, Professor Santosh Pandey and Professor Liang Dong, for their guidance and support throughout the course of this research.

In addition, I would also like to thank my friends and colleagues for making my time at Iowa State University a wonderful experience. A special thanks to Jingxiang Zhang for discussing some research problems with me and creating a productive lab environment. Finally, I must express my very profound gratitude to my families for providing me with unfailing support and continuous encouragement throughout my years of study and through the process of researching and writing this thesis. This accomplishment would not have been possible without them.

ABSTRACT

The main objective of this study is to develop a near-infrared (NIR) tunable external cavity laser (ECL) that is based on a semiconductor optical amplifier and two different wavelength selective elements. In order to achieve the wavelength selection, several filters have been tested in the ECL setups, including plasmonic filter, acousto-optic tunable filter (AOTF), gradient photonic crystal and Fabry-Perot (FP) cavity filter. The results show that the AOTF and FP filter have been applied successfully in the ECL system as wavelength selective elements to demonstrate a broadband wavelength tuning in the range between 830 nm and 870 nm. The tunable ECL realized with the variation of electrical radio frequency input of AOTF or incident angle of FP cavity filter from 15.5° to 30° in each system. By controlling the wavelength selective elements, continuous tuning of ECL over 30 nm can be achieved and 23 lasing peaks were measured and analyzed in the laser system with FP cavity filter. The characteristics of the AOTF-based and FP-based tunable ECL, including I-V curve, threshold, tuning range and output power, are measured and reported in this thesis.

Key words: tunable laser, external cavity laser, Fabry-Perot, acousto-optic, ring laser,

CHAPTER 1. INTRODUCTION

1.1 Organization of the Thesis

To develop tunable external cavity lasers (ECL) based on wavelength selective elements, it is important to understand the principles of filters and other parts of laser systems. The goal of this study is to examine wavelength selective filters and utilize them to construct a tunable external cavity laser with a wide spectral range in near infrared region.

Chapter 1 describes the fundamentals of tunable lasers, external cavity lasers and semiconductor optical amplifiers (SOA). Brief history backgrounds and developments of those devices are presented followed by introductions of laser components. A figure is shown in this chapter to provide a complete understanding of the mechanisms of SOA. Chapter 2 and Chapter 3 discuss two different wavelength selective elements for tunable lasers. Chapter 2 describes the tunable external cavity ring laser with the acousto-optic tunable filter (AOTF). The AOTF development and mechanisms, such as the piezoelectric effect and the acousto-optic effect, are introduced. All laser components and their functions are illustrated with some figures and tables. The results of the analyses is described in detail. Chapter 3 highlights the second wavelength selective element, the Fabry-Perot (FP) cavity filter. The focus of this chapter is on the principle of Fabry-Perot interferometer and cavity. Some equations are presented to show how this filter worked

as an optical filter. The fabrication details of this filter are also indicated. Results and discussions are contained to show the tunable process and the characteristics of Fabry-Perot cavity filters. Chapter 4 discusses the conclusions of this study. Some directions for future work in this area are also suggested.

1.2 Introduction of Lasers and Tunable Lasers

A laser usually consists of an optical resonator (cavity), and a gain medium. The circulating light can be amplified by the gain medium, thus compensating the loss of energy with high gain. However, the gain medium requires to be pumped electrically or optically, which based on different injections.

Tunable lasers allow output wavelengths tuning in specific spectral ranges from a few nanometers to hundreds of nanometers. All types of laser gain media are able to shift their wavelengths, but the tunable lasers give chances to shift their output wavelengths over broadband wavelength ranges. There are many types of tunable lasers with different controlled manners including broadly tunable lasers and narrow linewidth tunable lasers. The first broadly tunable laser, the dye laser, was introduced by P. P. Sorokin and F. P. Schäfer in 1966 [1][2] and the first narrow linewidth tunable laser was introduced by Hansch in 1972 [3].

In some cases, a particularly broadly tunable laser is required, whereas some other narrow band tunable lasers are desired in particular cases. The broadly tunable lasers, such as some solid-state bulk lasers (titanium–sapphire lasers) and dye lasers, offer tuning the output wavelengths ranging for hundreds of nanometers. The output power of those solid-state bulk lasers can be hundreds or even thousands of milliwatts. Despite the

rapid development in semiconductor laser technology, solid-state lasers still play a significant role in science, industry, and daily life [4].

Other types of lasers, such as the rare earth doped fiber lasers and laser diodes, allow adjusting the output wavelengths spanning a few nanometers to tens of nanometers. The tuning ranges for most of laser diodes is a few nanometers. However, external cavity lasers are able to adjust the output wavelength of 40 nm or more.

1.3 Introduction of External Cavity Lasers

External cavity lasers have been investigated for many years since they were introduced and demonstrated in 1964 [5]. External cavity lasers have the ability to select single output wavelengths from the entire output spectrum of the semiconductor optical amplifiers. There are a variety of ECL models that aim to adjust the output wavelengths within a wide range on the optoelectronic market. External cavity lasers introduce various new features, including narrowed line width and tunable wavelength. Figure 1.1 is the Littrow configuration which consists of a laser diode, a lens, and the diffraction grating.

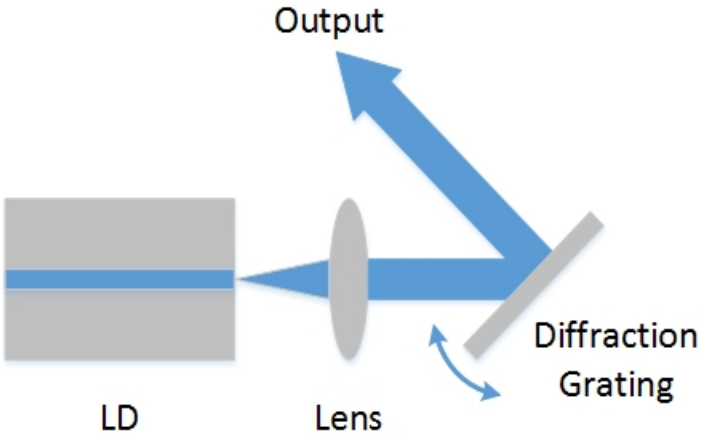

Figure 1.1 Structure of external cavity laser

Traditional intra-cavity lasers have wider line widths than other lasers, because intra-cavity lasers have smaller cavities that increase the frequency separation of two neighboring modes, $\Delta\nu_m = \nu_{m+1} - \nu_m = \nu_f$. The light frequency and wavelength are related by $\lambda=c/\nu$ in vacuum, and ν_m is the corresponding frequency for each mode, called the resonant frequency of the cavity. The free spectral range, also known as ν_f, impacts $\delta\nu_m$ by equation $\delta\nu_m = \nu_f / F$. F is a constant that is related to the reflectance R. When cavity length (L) increases, spectral width ($\delta\nu_m$) also increases as $\nu_f = c / 2L$. Therefore, intra-cavity lasers have larger bandwidths required to be narrowed by putting cavities outside of the SOA to provide narrowband optical feedback.

This study will focus on an external cavity laser with a ring configuration incorporating an acousto-optic tunable. The frequency selective element for this system is offered by the acousto-optic tunable filter or the Fabry-Perot filter and the spectral range for this system is near-infrared, from 840 nm to 870 nm.

1.4 Introduction of Semiconductor Optical Amplifiers

Semiconductor optical amplifiers are one kind of optical amplifier based on the electron-hole recombination in a semiconductor chip. This type of amplifiers uses a semiconductor to provide gain medium and has a similar structure to the laser diode [7]. The main difference between SOAs and laser diodes is that SOAs have anti-reflection (AR) coatings on the end faces as shown in Figure 1.2, which can reduce the end face reflection to less than 0.001%. Since there is no cavity in the SOA, loss of power that resulting from the anti-reflection coatings prevents the SOA to be a laser.

The SOA that worked in our system is called the traveling wave (TW) semiconductor optical amplifier. There are anti-reflection coating at the ends of the optical cavity so that the optical cavity does not act as an efficient optical resonator, a condition needed for laser oscillations [8]. Typically, semiconductor optical amplifiers are made of group III-V compound semiconductors such as GaAs/AlGaAs, because they have direct band gaps to satisfy the requirement that the probability of radiative recombination should be sufficiently high; in other words, there is enough gain at low current [9]. They are usually used in optical telecommunication systems in which the operating wavelength is between 850 nm to 1.6 μm.

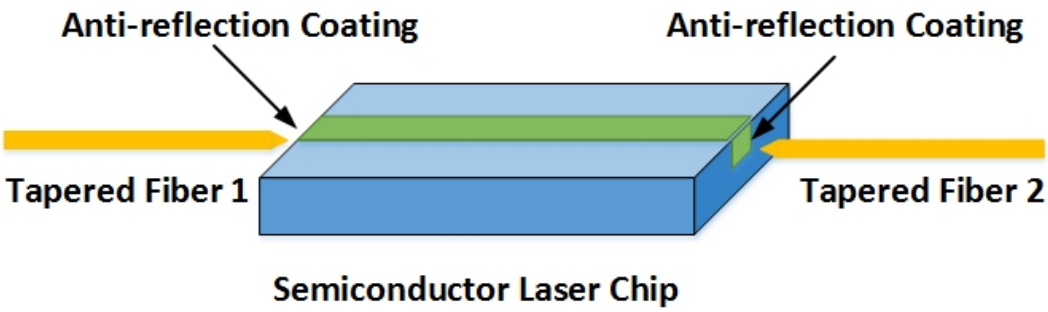

Figure 1.2 Structure of semiconductor optical amplifier

The reason that SOAs have been used widely in industry is that SOAs are not only cheaper but also smaller than the doped fiber amplifiers, such as the Erbium Doped Fiber Amplifier (EDFA), where the core is doped with trivalent erbium and the gain is in the 1550 nm region. However, compared with the EDFA, SOAs have low gain and high noise. One advantage of SOAs is that they can be pumped electrically by low power systems [10]. High power may cause nonlinear effects in the fiber or overload the

receiver when an EDFA is used by a wavelength-division multiplexing (WDM) system to transmit signals. As there is no ‘‘mirror’’ structure on the end faces of semiconductor optical amplifiers, researchers can drive the light out of SOAs and make it through the external cavity that we set up. After that, wavelength selective elements are used to tune the wavelength desired.

CHAPTER 2. TUNABLE EXTERNAL CAVITY RING LASER WITH ACOUSTO-OPTIC TUNABLE FILTER

2.1 Introduction of Acousto-Optic Tunable Filters

By using the acousto-optic tunable filter (AOTF) for the wavelength selectivity in the external cavity of a SOA, wavelength tuning is realizable in a wide spectral range. The acousto-optic tunable filter that consists of a piezoelectric transducer bonded to a birefringent crystal is based on the acousto-optic effect to diffract the frequency of incident optical radiation. A researcher can determine the wavelength of diffracted light by changing the electrical input of the radio frequency (RF) of the transducer [6]. The spectral range that AOTF can drive ranges from visible to mid-infrared with different types of acousto-optic tunable filters. There are two kinds of acousto-optic tunable filters in terms of configurations, quartz collinear AOTF and tellurium dioxide (TeO_2) non-collinear AOTF. In collinear AOTF, the incident light, the diffracted filtered light and the acoustic wave interact collinearly in the crystal. A narrow band of spectral wavelengths is diffracted into a polarization direction that is orthogonal to the incident beam. Behind the quartz crystal, an output polarizer is utilized to separate the narrowband diffracted light from the coupled collinear beam. The filter that is used in our work is the Tellurium Dioxide non-collinear (350-5000 nm) AOTF that operates in the near-infrared region. In this non-collinear design, the diffracted beam and the un-diffracted beam are separated

into different angles, because the acoustic and optical waves propagate with fixed angles after they leave the crystal.

When the transducer is excited by the AOTF driver with an electrical RF wave, an acoustic wave will be stimulated in the acousto-optic crystal. Then the crystal generates a periodic variation of the refractive index, which enables the crystal to diffract part of the incident light in some specific conditions [11]. For a fixed frequency, only a narrowed band of incident light satisfies the special condition. When researcher adjusts the input frequency on the control system, the wavelength of diffracting light also changes accordingly.

The piezoelectric effect is the ability for a certain material to convert applied mechanical energy into electrical energy. The word Piezoelectric is derived from the Greek word “piezen”, which means squeeze or press. What is important is that the piezoelectric effect is reversible, meaning that the material exhibits the conversion of applied mechanical energy into electrical energy also exhibits the conversion of applied electrical energy into mechanical energy (converse piezoelectric effect). By applying mechanical pressure on a quartz crystal along a certain plane, generation of electrical polarity is available to realize. There are two types of physical stress can be converted, including compressive stress and tensile stress and they are shown in Figure 2.1.

The piezoelectric transducer is a transducer that can convert energy from one form into another. By applying an oscillating electrical radio frequency signal, the piezoelectric transducer converts electrical pulses into mechanical vibrations, which result in a periodic variation of refractive index through the crystal. The piezoelectric transducer comprises of quartz crystal that is made from silicon and oxygen in crystalline

structure (SiO_2). The piezoelectric crystals in the transducer are electrically neutral. The atoms inside the piezoelectric crystals are not symmetrically arranged but their electrical charges are balanced (positive charges cancel out negative charge). Due to the piezoelectric effect, the piezoelectric transducers in AOTF are able to convert an oscillating RF wave into an acoustic wave and the corresponding driving frequency ranging from tens to hundreds of megahertz. Piezoelectric transducer apply an oscillating electric field to create a mechanical wave, which changes the refractive index by propagating through the crystal.

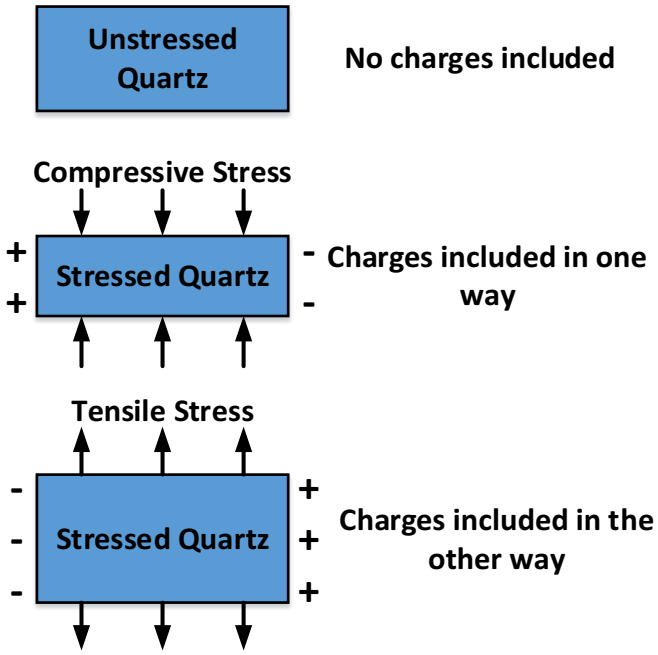

Figure 2.1 Principle of the piezoelectric effect

The acousto-optic effect, also known as the acousto-optic interaction or diffracting of light by acoustic waves, was first introduced by Brillouin in 1921 [12], and demonstrated by Biquard and Sears in 1932 [13][14]. This effect is produced by

stimulating an acoustic wave in an optically transparent material. The ultrasonic wave results in a periodic variation of refractive index in acousto-optic crystal. As the periodic variation of refractive index, the medium is similar with a diffraction grating, which spacing is determined by the wavelength of acoustic wave. When the transducer is excited by the AOTF driver, the acousto-optic crystal is deformed by the application of electric field. This deformation produces an internal strain which is transmitted into the crystal that is bonded to a piezoelectric transducer. Any strain in crystal should generate a change in the refractive index and finally results in the diffraction of incident light. In a case of this effect, the strain is produced by an acoustic wave that generated in crystal. Thus, we could say that acoustic wave is accompanied by refractive index variations. Piezoelectric acoustic wave apply an oscillating electric field to create a mechanical wave, which changes the refractive index by propagating through the crystal.

Table 2.1 AOTF technical parameters.

Model	TEAF_-.55-1.0_
Spectral Range (nm)	550-1000
Drive Freq.(MHz)	155-70
Optical Aperture(nm)	5.0 x 5.0
Spectral Resolution(nm)	1.5-8.3(S) 0.9-5.0(H)
Acceptance Angle(degree)	4.3-5.9(S) 3.2-4.5 (H)

The AOTF that used in this study is based on the acousto-optic effect to diffract the frequency of the incident light by using acoustic waves. The Brimrose Acousto-Optic Tunable Filter is a solid state acousto-optic device with no moving parts. It functions as a

tunable acousto-optic filter that separating a specific frequency from a broadband laser source. The AOTF is able to precisely and rapidly adjust the wavelength by using the controller system, including the AOTF driver and the computer. AOTFs are used widely in numerous optical systems and applications, especially in industrial or process control, such as the NIR spectroscopy applications [15].

2.2 Laser Components and Design

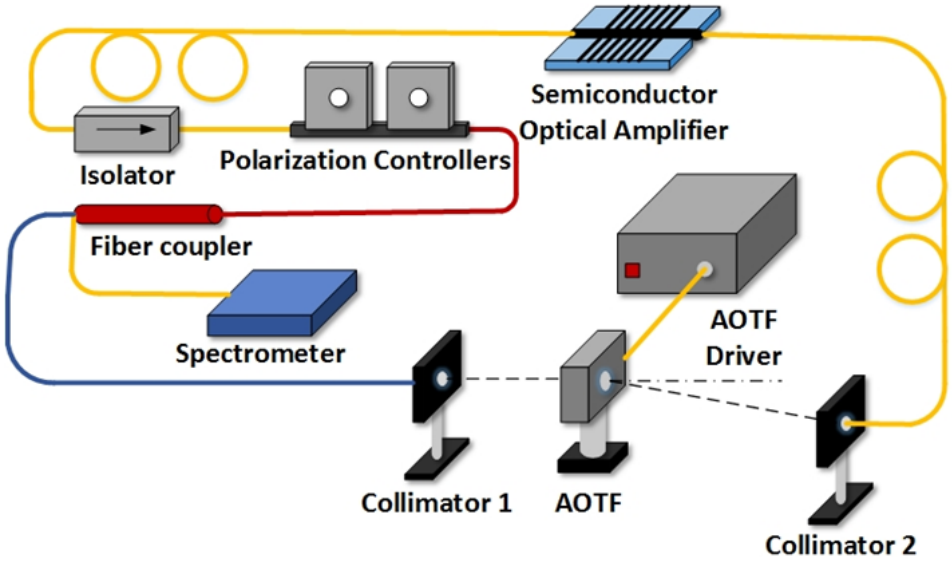

Figure 2.2 Scheme of Tunable external cavity ring laser with acousto-optic tunable filter

Figure 2.2 shows the design of tunable external cavity ring laser with the acousto-optic tunable filter. The tunable laser is made by a NIR semiconductor optical amplifier and an acousto-optic tunable filter between two optical collimators. When semiconductor optical amplifier emits light, the isolator is used to stabilize the laser system and block light beam that coming from the right side of SOA. The polarizer is utilized to adjust the

polarization of light beam and maximize the energy that coupled by collimator 2. In order to observe the energy in cavity, part of energy is coupled by the beam splitter and transmitted to spectrometer in the end. The fiber collimator 1 is in charge of collimating light from single-mode fiber with diffraction-limited performance. The selected light beam is diffracted by the AOTF with a specific angle. Besides AOTF, there is a driver that controlling the electrical RF signals. The transmission peaks can be selected by this setup to tune the external cavity laser. The diffracted wavelength that is collimated by the fiber collimator 2 returns to the semiconductor optical amplifier on the other end as the optical feedback.

Table 2.2 Isolator technical parameters [16].

Item #: IO-F-850	
Polarization	Independent
Fiber Type	SM
Center Wavelength	850 nm
Operating Range	840 - 860 nm
Max Power	2 W (CW)
Isolation	≥30 dB
Insertion Loss	≤1.6 dB
Polarization Dependent Loss	≤0.25 dB
Return Loss	≥50 dB

The isolator that worked in this system, also known as the Faraday isolator or the polarization-independent isolator, is used to absorbing or displacing the light sources near 850 nm from the reverse direction and then stabilize the tunable laser system, because opposite signals increase noise intensity and optical damage. The polarization

independent isolators mainly consist of three parts, an input birefringent wedge, a Faraday rotator and an output birefringent wedge. Light traveling in both directions are split into two beams at the first wedge, but the forward light recombine in output wedge, whereas the backward light diverge.

The manual fiber polarization controller can produce stress-induced birefringence by wrapping the fiber around two spools to alter the polarization of light. There are two paddles providing two independently rotatable wave plates and each paddle provides 143° of rotation. The function of the manual fiber polarization controller is to adjust the polarization of the light before light beam traveling through the AOTF. As the acousto-optic tunable fiber is able to diffract fixed wavelength to a fixed angle with different polarized direction, we can rotate two paddles on the polarization controller to change the ratio of TM mode to TE mode and minimize the power of plus one order which collimator 2 was collecting.

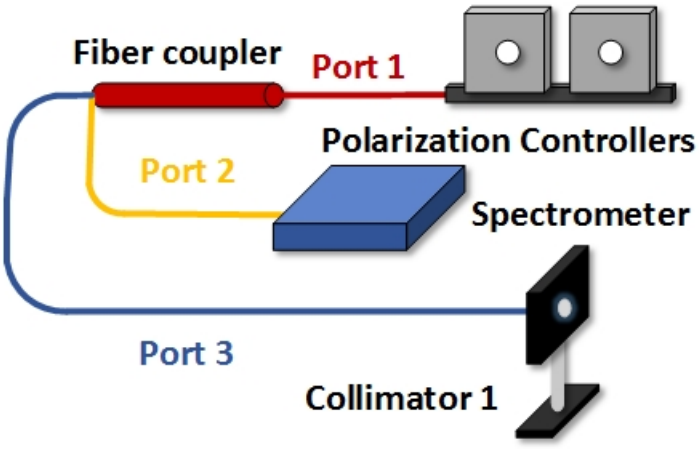

Figure 2.3 Scheme of fiber coupler with three ports

The fiber Coupler that worked in this system has three ports as showing in Figure 2.3. Port 1 is connected to the polarization controller to receive the light beam from the SOA. It functions to split the beam into two beams by 50% to 50%. Port 2 that carries 50% power from port 1 is connected with the spectrometer to analyze optical spectrum of the laser system. Port 3 is used to transmit another 50% of power into collimator 1 and finally return to the right side of the semiconductor optical amplifier as optical feedback. Figure 2.3 shows the scheme of the fiber coupler that is used in this work. The port 1 is shown in red line, the port 2 is shown in yellow line, and the port 3 is shown in blue line. The light beam were separated into 2 beams by the 50:50 fiber coupler.

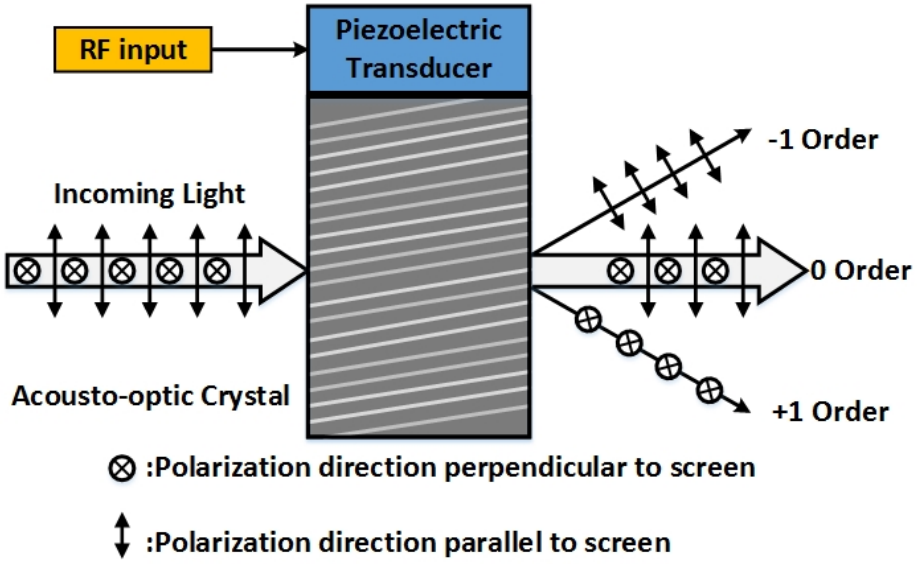

Figure 2.4 Acousto-optic tunable filter consists of acousto-optic crystal and piezoelectric transducer. Incoming beam is diffracted into different orders.

The AOTF acts as a wavelength selective element and tunes the output wavelength by continuous inputting the electrical RF signals into piezoelectric

transducer. The light beam is separated into different beams after it went through the acousto-optic crystal in AOTF. The zero order is the ordinary one that has the same direction with the input beam. However, there are two first orders, one is the plus and the other is the minus. Both the plus and minus first order can select the wavelength with orthogonal polarization directions, but the plus first order is the order that is maximized by the manual fiber polarization controller and has stronger power than minus first order. Therefore, minus first order can be omitted because of its negligible power comparing with the plus first order.

Due to the birefringence of the acousto-optic crystal, un-polarized incident light is divided inside the crystal into ordinary and extraordinary polarized light. [17] The piezoelectric transducer that stimulated by radio frequency waves generates the acoustic waves in the crystal. The incoming un-polarized light interacts with this acoustic waves in acousto-optic crystal and diffracts the light beam with the corresponding wavelength. As showing in Figure 2.4 above, un-polarized incident light comes in from left side and interacts with acoustic waves in the crystal. Thus, plus first and minus first order are separated from the incoming light with different polarized directions. The plus first order wave is the ordinary wave and the minus first order wave is the extraordinary wave. We are able to maximize energies in ordinary wave or extraordinary wave by rotating the paddles of the manual fiber polarization controller as mentioned above.

There is a relationship between the selected wavelength, incident angle, sound wave velocity and driving frequency [18]. For the acousto-optic anisotropic medium, λ is the wavelength of diffracted light, V_a is the velocity of the acoustic wave, f_a is the radio frequency and θ is the incident angle. The accurate equation for λ and f_a is:

$$\lambda = \left[V_a \Delta n (\sin^4 \theta_i + \sin^2 2\theta_i)^{1/2}\right]/f_a \quad (2.1)$$

As we can both see through equation (2.1) and Table 2.3, the wavelength of diffraction light decreases when increases radio frequency. In this equation, Δn is the absolute difference between ordinary and extraordinary refractive index.

2.3 Output Characteristics of the Tunable Laser

Figure 2.5 gives the emission spectrum of the SOA and the ECL with AOTF for the injection current of 75 mA. The blue line represents the stimulated emission of the ECL with AOTF and the red line represents the spontaneous emission of the SOA. The central wavelength of the ECL with AOTF was tuned to the 858.2 nm, corresponding to the RF of the AOTF driver (87 MHz) and the laser linewidth was observed as narrow as 0.5 nm with the spectrometer.

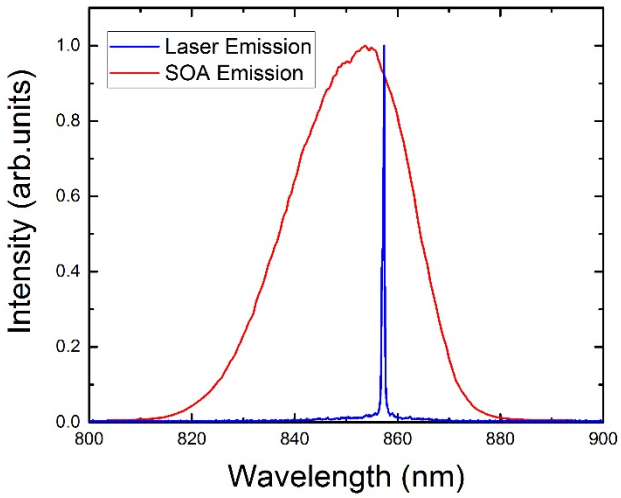

Figure 2.5 Emission spectrum of semiconductor optical amplifier and external cavity laser with acousto-optic tunable filter as central wavelength of 857.9 nm

Figure 2.6 shows the output optical power versus injection current at the AOTF operating frequency of 88 MHz. The blue dots represents the stimulated emission of the ECL with AOTF and the red dots represents the spontaneous emission of SOA. The thresholds for ECL with AOTF are different at each RF frequency that is controlled by AOTF driver and the output power of the laser can as high as 8mW when the injection current reaches 80 mA.

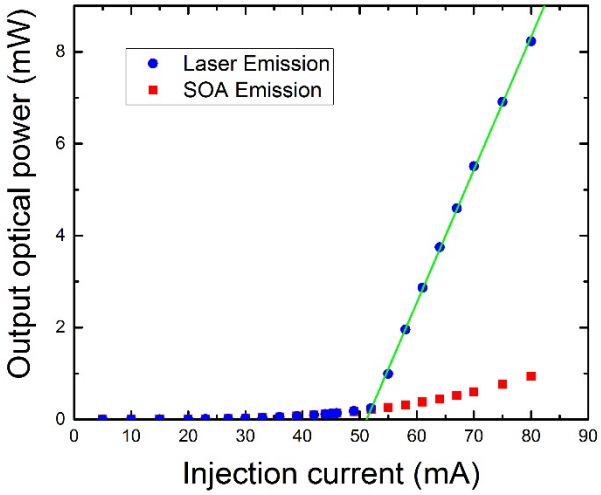

Figure 2.6 Power-current characteristics of semiconductor optical amplifier and external cavity laser with acousto-optic tunable filter at operating frequency of 87 MHz

The thresholds of this laser system reach its lowest when tunes the frequency of AOTF to 87.5 MHz. The ECL with AOTF is dominated by spontaneous emission when the injection current is below its threshold. However, the output power begins to grow rapidly when its injection current increases beyond threshold, which means it starts to lase. Obviously, output optical power increases rapidly in the lasing region but remain

slowly increases below threshold. When the threshold is higher than 52 mA, there is a distinct difference between laser emission (stimulated emission) and spontaneous emission that can be observed on Figure 2.6. The optical feedback in laser system results in this distinction between the SOA emission and laser emission. The green straight line which shows the threshold of this laser is the linear fitting of stimulated emission.

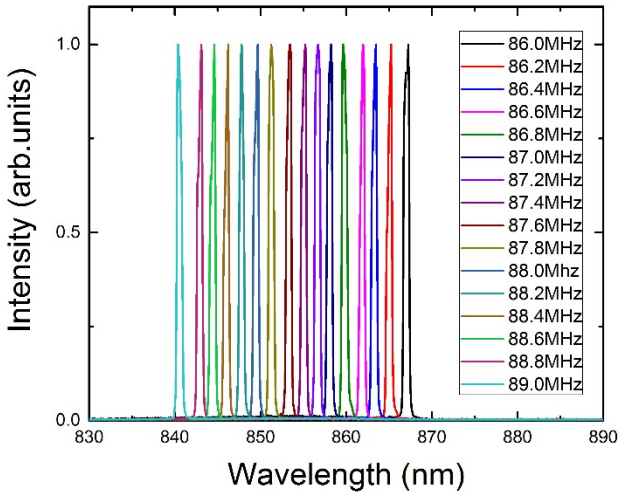

Figure 2.7 External cavity lasing spectrum with each acousto-optic tunable filter frequency

Figure 2.7 shows that the different peaks of external cavity laser when tunes the electrical radio frequency of the AOTF driver. As we can see in this figure, there are 16 peaks available for tuning between 840 nm and 867 nm and the peaks showing on screen are quite stable and sharp. In theory, the laser can be tuned every 0.1 MHz and each frequency corresponds to one peak, which means that over 32 peaks can be found in this laser system. We just adjusted the frequency every 0.2 MHz and each frequency gives a specific central wavelength as shown in different colors. Therefore, we can tune this ECL continuously and smoothly. In the Figure 2.7, the shortest wavelength is 840.4 nm

corresponding to the radio frequency of 89 MHz and the longest wavelength is 867.2nm corresponding to the radio frequency of 86 MHz.

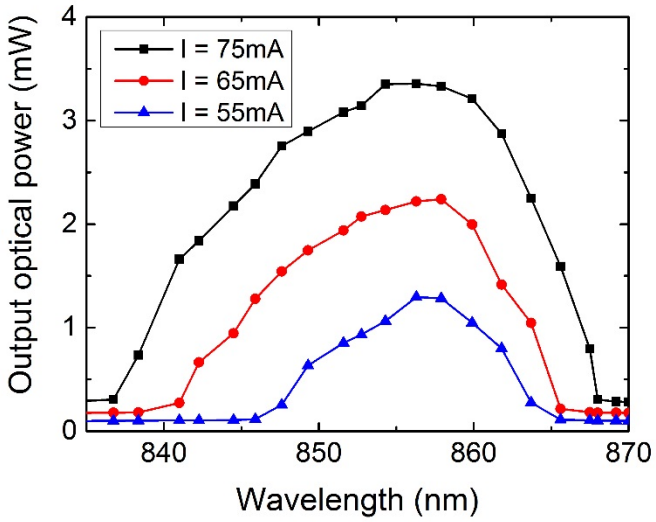

Figure 2.8 Output optical power in automatic current control mode at different injection currents

Figure 2.8 provides the variation of laser tuning curves in the automatic current control (ACC) system. Figure 2.8 shows that the tuning range for the ECL with AOTF broadens as we increases the injection current. The output optical power reaches its highest point at corresponding central wavelength and lowest below lasing threshold at each electrical radio frequency. The black, red, and blue dots show the variation of output optical power under the ACC system with 75 mA, 65 mA, and 55 mA, respectively. In conclusion, the tuning range broadens with the increase of the injection current, and the output optical power increases with the increase of the injection current as well, because of the corresponding broadening of the SOA gain band.

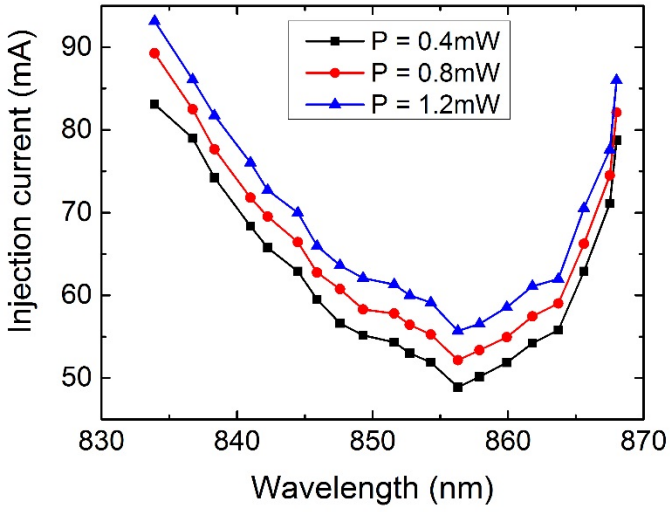

Figure 2.9 Injection current in automatic power control mode at different output powers.

Figure 2.9 provides the variation of laser tuning curves in the automatic power control (APC) system. The tuning range for the ECL with AOTF narrows down as we decrease the output optical power. The injection current that is required to fix output power reaches the lowest point at the corresponding central wavelength and the highest below the lasing threshold at each electrical radio frequency. The black, red and blue dots show the variation of the required injection current under the APC system with 0.4 mW, 0.8 mW and 1.2 mW respectively. In conclusion, the lower the output power, the broader the tuning range and the lower the injection current. The tuning range broadens with the increase of the output power, and the injection current increases with the increase of output power as well, because of the corresponding broadening of the SOA gain band.

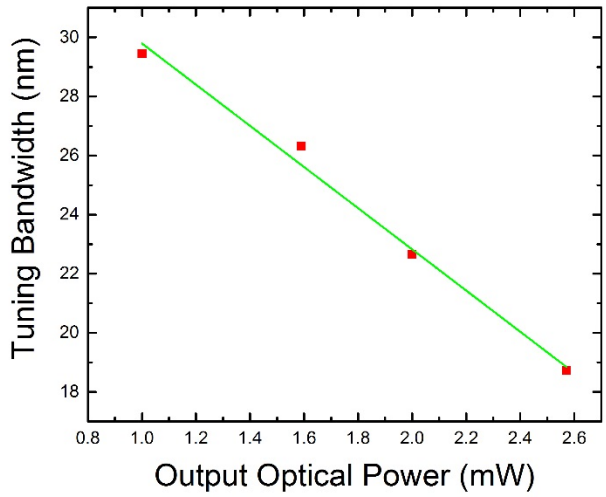

Figure 2.10 Tuning range width versus output optical power

Figure 2.10 above shows the tuning range width curve. As we discussed on the last figure, tuning bandwidth decreases from the highest point to the lowest with an increase of output optical power in the APC system.

Table 2.3 Corresponding ECL lasing wavelengths with the operating frequency of acousto-optic tunable filter

Wavelength (nm)	Frequency (MHz)	Wavelength (nm)	Frequency (MHz)
867.2	86	853.5	87.6
865.2	86.2	851.2	87.8
863.5	86.4	849.7	88
861.9	86.6	847.6	88.2
859.6	86.8	846.2	88.4
858.2	87	844.6	88.6
856.7	87.2	843.1	88.8
855.2	87.4	840.4	89

Table 2.3 shows the corresponding ECL lasing wavelengths with each operating frequency of acousto-optic tunable filter. The tunable spectral range is between 840 nm

and 867 nm. When researcher changes the frequency on computer, a corresponding acoustic wave is created in the acousto-optic crystal and the selected wavelength is diffracted by this wave.

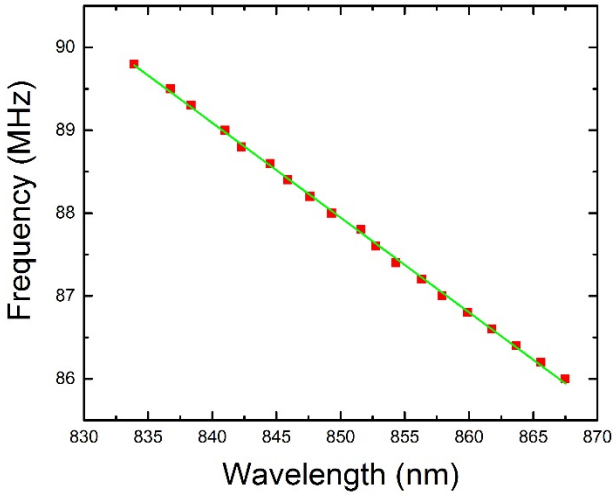

Figure 2.11 Wavelength (λ) varies with radio frequency (f_a)

Based on the collected data, there is a relationship between selected wavelength and driving frequency as shown in Figure 2.11.

$$Y=1618.36-8.74*X \tag{2.2}$$

Where X is the radio frequency and Y is wavelength. In conclusion, a fixed frequency corresponds to a fixed selected wavelength in the acousto-optic crystal.

2.4 Summary for Tunable Laser with Acousto-Optic Tunable Filter

A tunable external cavity laser using an acousto-optic tunable filter and a semiconductor optical amplifier was proposed and demonstrated. The output wavelength of the ECL was determined by the electrical radio frequency that driven by the AOTF driver. As the wavelength selective element for this ECL system, AOTF tunes the lasing range from 840 nm to 867 nm. By controlling the wavelength selective elements, continuous tuning of ECL over 27 nm can be achieved and 16 lasing peaks were measured and analyzed in the laser system with the AOTF filter. The tuning range of this tunable laser can be easily extended by increasing the injection current.

CHAPTER 3. TUNABLE EXTERNAL CAVITY RING LASER WITH FABRY-PEROT CAVITY FILTER

Continuous tuning over a 32 nm region in the NIR region was achieved with an external cavity ring laser that mainly consists of a semiconductor optical amplifier and a Fabry-Perot cavity filter. In a departure from traditional external cavity lasers, the wavelength selective element for this laser system is provided by the Fabry-Perot cavity filter that confines and stores the energy of light at a selected wavelength. The Fabry-Perot cavity filter used in this study was fabricated by gilding it with gold and coating it with thin polymer film.

3.1 Introduction of Fabry-Perot Cavity Filters

Charles Fabry and Alfred Perot discovered the Fabry-Perot filter at the University of Marseille in 1897 [19]. With this work, an optical phenomenon called resonance was discovered. This discovery resulted in the invention of an effective way to measure small distance. In 1902, Fabry and Perot established the principle of interference between two plates. Several measurement techniques that are based on this principle were applied in labs across Europe. Recently, FP filters have been mainly used in sensors and measurement applications. Vails and his colleagues have demonstrated the use of FP filters as in-fiber mirrors for the measurement of strain [20]. The FP filters have also

found applications in medical fields as blood pressure and temperature sensors by Van Brakel [21].

As optical resonators are able to store light energy in selected wavelengths or frequencies, an FP filter mainly consists of two parallel planar mirrors spaced a fixed distance apart. There are several tuning mechanisms for Fabry-Perot filters such as adjusting plates spacing, changing the refractive index, and tilting the filter to different angles. The tuning mechanism for the Fabry-Perot filter used in this study is to change its incident angle. Thus, tuning wavelengths can be realized by tilting the filter and changing the incident angle of the NIR light.

The FP filter is an optical resonator that has an FP cavity structure-a sandwich structure with two gold nanostructures metal layer and one SU-8 polymer layer. A gold nanostructure coating process was used to fabricate this Fabry-Perot filter with an optical resonance pattern. In this process, a cover slip was utilized as the substrate to create the ideal Fabry-Perot structure. The first step, a nanostructure layer of gold was coated on the cover slip in our lab. Next, the sample was coated with an SU-8 polymer by spinning the slab at selected speed and time. In order to make sure that the surface was as flat as possible, baking and melting were significant for the sample. Finally, another nanostructure layer of gold was required to complete the whole process.

Fabry-Perot cavity filters are ideal optical materials for controlling light propagation with different incident angles. The transmission peaks of the FP filter can be tuned by manipulating the stage controller to tilt the filter in different incident angles. It means that Fabry-Perot cavity filter has different transmission peaks with different incident angles. Therefore, as an effective wavelength selective elements, Fabry-Perot

cavity filters can be used to filtrate incoming light within the NIR region in external cavity laser system.

3.2 Design and Laser Components

Figure 3.1 shows the design of the tunable external cavity ring laser with the Fabry-Perot cavity filter. The tunable laser is mainly made by the NIR semiconductor optical amplifier and the Fabry-Perot cavity filter between two optical collimators.

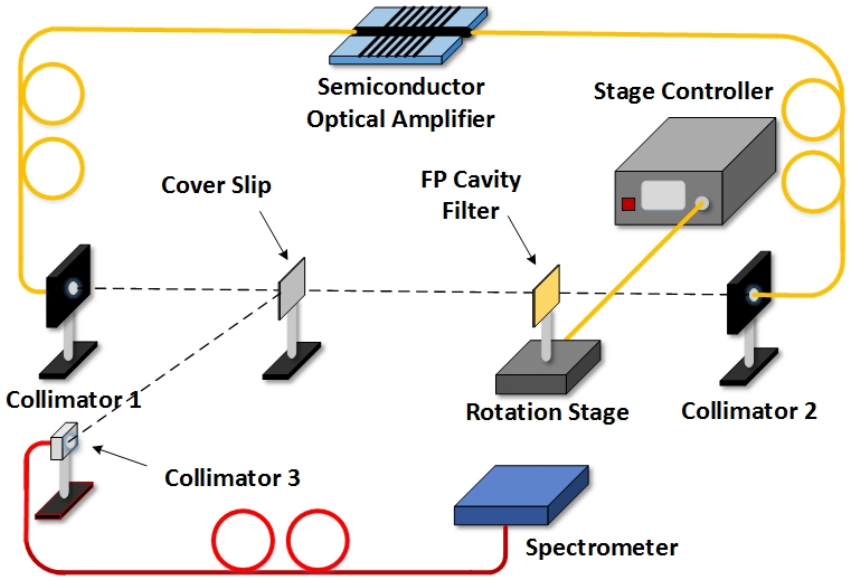

Figure 3.1 Scheme of Tunable external cavity ring laser with Fabry-Perot cavity filter

When semiconductor optical amplifier emits light, the fiber collimator 1 is in charge of collimating light from single-mode fiber with diffraction-limited performance. The cover slip in the cavity is used to reflect part of the light beam that coming from the fiber collimator 1. This part of light energy is collimated by the fiber collimator 3 and transmitted to the spectrometer in order to analyze energy in the cavity. The remaining

light energy passes through the cover slip and reaches the Fabry-Perot cavity filter. The FP filter is an optical resonator that confines energy in the selective wavelength. Below the FP cavity filter, there is a rotation stage that connecting with a stage controller. The incident angle can be controlled by this setup to move transmission peaks. The selected wavelength light crosses Fabry-Perot cavity filter and is collimated by the fiber collimator 2. This selected light returns to semiconductor optical amplifier on the other end as optical feedback.

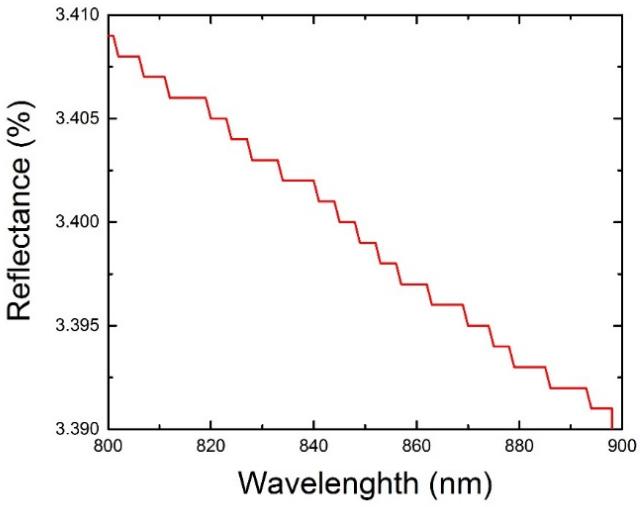

Figure 3.2 Reflectance of cover slip varies with wavelength

The cover slip is a thin flat square transparent glass with 20 mm. It is usually utilized to place over objects for viewing under the microscope in laboratories. There are two cover slips in this system with different functions. The first one is used to reflect part of the light beam that coming from the fiber collimator 1. For the SOA that worked in this thesis, the reflectance ranging from 3.395% to 3.403% as shown in Figure 3.2. The

power that is collimated by the fiber collimator 3 is just small part of total cavity power. It is convenient to calculate the total power by utilizing the figure above.

The fiber collimators (FC) are aligned to collimate light from a single mode fiber into a free-space collimated beam with diffraction-limited performance. Due to chromatic aberration, the lens in fiber collimator is unable to focus all the wavelengths of color to the same focal plane. Chromatic aberration results from the lens dispersion, with different wavelengths of light transmitting at different speed while passing through the lens. The designed wavelength for fiber collimator indicates the wavelength of the ideal beam.

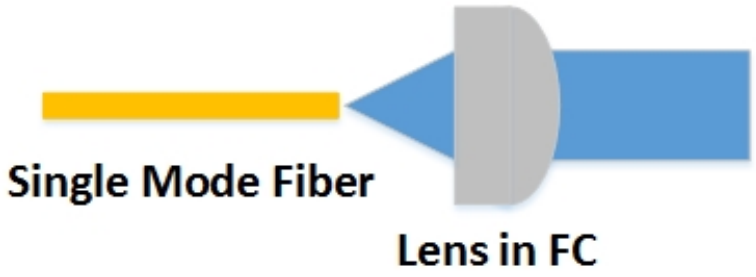

Figure 3.3 Lens in fiber collimator collimate light from fiber

Fiber collimator 1 can collimate the output from single mode fiber, and then launch a collimated beam into another single mode fiber by fiber collimator 2. The lens has AR coating on both sides that minimizes the reflections from the surface. Collimators are designed to work best with single mode fibers but also works with multimode fibers. Collimator mounting adapters that can adjust incident angles and positions are used for collimator 1 and 2 to mount fiber collimation in our work.

3.3 Fabrication of the Fabry-Perot Cavity Filter

Fabry-Perot filters are well-known for playing a significant role in the fields of sensors and measurement applications. [8] Fabry-Perot filters have also been widely used in the optical field as the wavelength selective properties. We utilized those properties in our tunable laser system that requires narrow full width at half-maximum (FWHM) and wide free spectrum range (FSR). By adjusting the width of the photoresist layer, the free spectrum range can be easily broadened to an ideal range that fitting in the NIR spectroscopy. Due to the narrow output spectrum of SOA that ranging from 830 nm to 870 nm, we want a Fabry-Perot cavity filter with FSR around 30-40 nm, which means only one peak exists in this narrow region when tilts the sample to any incident angle. In order to get suitable FWHM, the thickness of gold coating must be thinner than 30 nm.

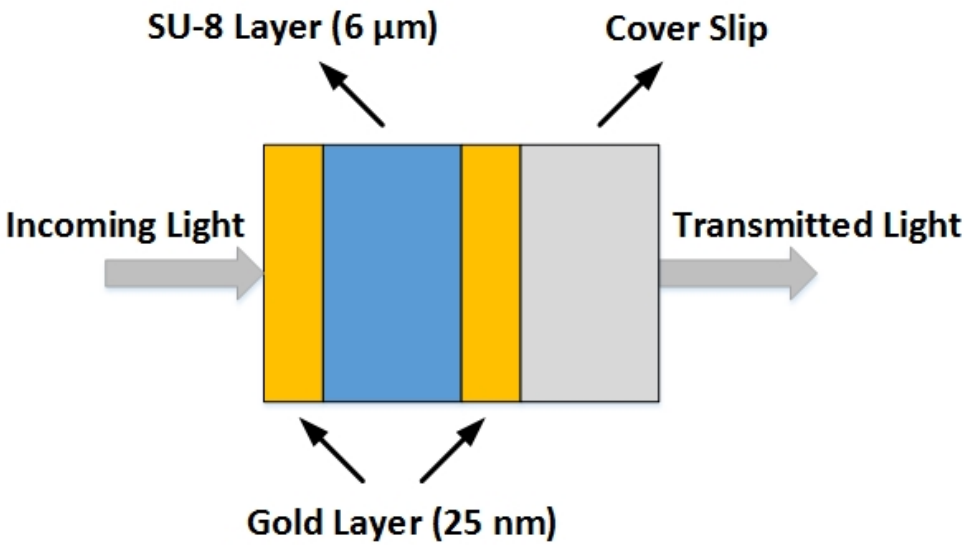

Figure 3.4 Fabrication of Fabry-Perot cavity filter

The FP filter is an optical resonator that has Fabry-Perot cavity structure -a sandwich structure with two gold nanostructures with 25 nm and one SU-8 layer with 6

μm. A gold nanostructure coating process is used to fabricate this Fabry-Perot filter with an optical resonance pattern. In this process, a cover slip was utilized as the substrate to create the ideal Fabry-Perot structure. First step, a nanostructure layer of gold is coated on the cover slip in our laboratory. Secondly, the sample was coated with an SU-8 polymer by spinning the slab at selected speed and time. In order to make sure the surface is as flat as possible, baking and melting are significant for the sample. Finally, another nanostructure layer of gold is required to complete the whole process.

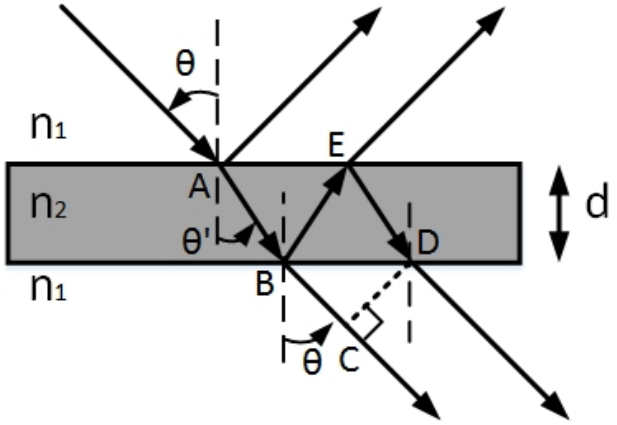

Figure 3.5 Path length difference of Fabry-Perot cavity filter

Figure 3.5 shows that the multiple reflections and refractions of the Fabry-Perot Filter result in the path length difference. We assume that there is a dielectric material (First dielectric material) with refractive index of n_2 surrounded by a material (Second dielectric material) with refractive index of n_1. The thickness of first dielectric material is d and the incident angle of the light beam is θ. When the incident light irradiates on the first interface of n_1 and n_2, part of light energy will be reflected at the first interface with an angle of θ, whereas the remaining part of light energy will be refracted into the first dielectric material with the angle of θ'.

The refracted energy will go through the first dielectric material and reach the second interface on the other side. Part of this energy will be reflected back at the second interface with an angle of θ', whereas the remaining energy will be refracted out of the first dielectric material with the angle of θ. There are multiple reflections and refractions between the interfaces of n1 and n_2 during this process and a number of secondary reflected and refracted beams with decreasing intensity. Due to the phase difference that shifting during this process, the refracted beams interfering constructively or destructively. Based on Figure 3.5, the optical path difference (δ) between two consecutive beams can be easily calculated

$$\delta = n_2(BE + ED) - n_1 BC \tag{3.2}$$

where

$$\mathrm{BE} = \mathrm{ED} = \frac{d}{\cos\theta'} \tag{3.3}$$

and

$$BC = BD \sin\theta \tag{3.4}$$

$$BD = 2\frac{d}{\cos\theta'}\sin\theta' \tag{3.5a}$$

$$BC = 2d \tan\theta' \sin\theta = [2n_2 d \sin\theta'^2 / \cos\theta']/n_1 \tag{3.5b}$$

Finally, the path length difference can be achieved by

$$\delta = 2n_2 d \cos\theta' \tag{3.6}$$

This path length difference (δ) results in the phase shift ϕ equal to

$$\phi = \frac{2\pi}{\lambda}\delta = \frac{4\pi}{\lambda} n_2 d \cos\theta' \tag{3.7}$$

where λ is the wavelength of light beam and d is the thickness of the middle layer.

The phase shift ϕ that be calculated from equation (3.7) is the phase difference between consecutive beams due to path length difference. In Figure 3.5, consecutive beams interfere constructively when experience even π phase shift, whereas beams interfere destructively when experience odd π phase shift. Assuming the incoming light is normally incident on the first surface, equation (3.7) can be simplified as

$$\phi = \frac{4\pi n_2 d}{\lambda} \tag{3.8}$$

The phase shift can also be expressed as a function of frequency (*f*)

$$\phi = \frac{4\pi n_2 df}{c} \cos\theta' \tag{3.9}$$

where c is the velocity of light in vacuum.

Consecutive beams interfere constructively when experience even π phase shift.

$$2\pi m = \frac{4\pi n_2 d}{\lambda} \cos\theta' \tag{3.10}$$

where m is the integer that represents the order of the transmission peaks existing in the FP filter.

As shown in equation (3.10), the phase shift is even π and we can simplify this as equation (3.11). The wavelengths of transmission peaks can be calculated by using equation (3.11) with different incident angles, the refractive index of n_2 and the layer thickness of d.

$$\lambda = \frac{2n_2 d}{m}\cos\theta' \tag{3.11}$$

The central wavelengths of two consecutive transmission peaks (λ_1 and λ_2) can be calculated with equation (3.12) and (3.13). The orders for those two consecutive transmission peaks are m and m+1.

$$\lambda_1 = \frac{2n_2 d}{m}\cos\theta' \tag{3.12}$$

$$\lambda_2 = \frac{2n_2 d}{m+1}\cos\theta' \tag{3.13}$$

Free spectral range (FSR) of the FP filter is the frequency spacing between two consecutive transmission peaks. Then the FSR in term of wavelength can be obtained by equation (3.12) and (3.13). Where m is an integer as mentioned before.

$$\Delta\lambda_{FSR} = \frac{2n_2 d}{m(m+1)}\cos\theta' \tag{3.14}$$

If m is larger enough, (3.14) becomes

$$\Delta\lambda_{FSR} = \frac{\lambda^2}{2n_2 d\cos\theta'} \tag{3.15}$$

By accurately setting the value of thickness (d) and incident angle θ', the desired FSR can be achieved in the FP cavity filter. The FSR in term of frequency can be expressed by equation (3.16) as $\Delta f_{FSR} = (c/\lambda^2)\Delta\lambda_{FSR}$ when $\Delta f_{FSR} << f$.

$$\Delta f_{FSR} = \frac{c}{2n_2 d\cos\theta'} \tag{3.16}$$

If the angle is normal incident, we approximate that $\cos\theta' = 1$. Then equation (3.15) becomes

$$\Delta\lambda_{FSR} = \frac{\lambda^2}{2n_2 d} \tag{3.17}$$

Finesse($\mathcal{F}$), the ratio of the FSR to the FWHM, is a significant parameter for FP cavity filter. Finesse indicates the number of beams that interfering in FP cavity to form the standing wave. The higher finesse value indicates the more interfering beams in the cavity.

$$\mathcal{F} = \frac{\Delta f_{FSR}}{\Delta f_{FWHM}} \tag{3.18}$$

The reflectance (R) of FP cavity mirrors is the primary factor to influence the finesse as shown in equation (3.19). It influences the number of beams that including the FP cavity.

$$\mathcal{F} = \frac{\pi\sqrt{R}}{1-R} \tag{3.19}$$

Equation (3.19) shows that the finesse can be higher by increasing the reflectance of FP cavity mirrors, but the increase of reflectance results in the low refraction of FP filter. In another word, the total energy that passing through the filter decreases as the growth of mirrors' reflectance. The gold coating is required in our work as its high reflectivity when it be coated over 25 nm, in order to achieve high contrast to perform wavelength selection.

As shown in Figure 3.6, the contrast between 800 nm to 900 nm is high enough to be the wavelength selective element in our system. The finesse for this FP cavity filter is as high as 19 based on the calculation of the equation (3.19). It is obvious that the contrast at 600 nm is higher than the contrast at 800 nm in Figure 3.6. As we can see in Figure 3.7 that there are different transmissions on different central wavelengths. Therefore, when the central wavelength (λ) increases, the reflectance (R) and the finesse

(F) also increases. The consequence of this increase in finesse results in the reduction of the transmissions in Figure 3.6.

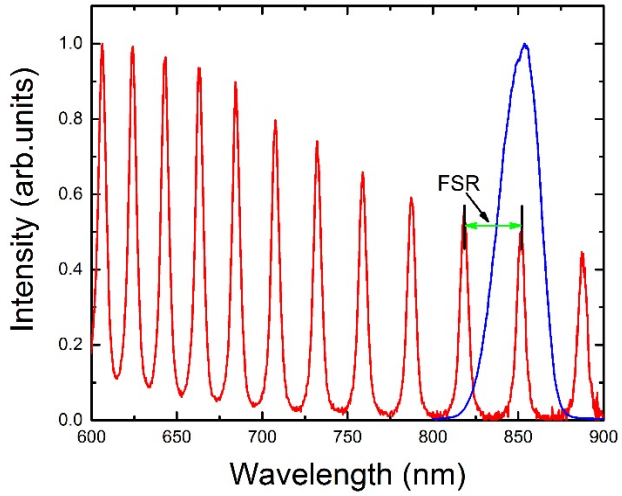

Figure 3.6 Fabry-Perot cavity filter Transmission Spectrum at normal incidence angle

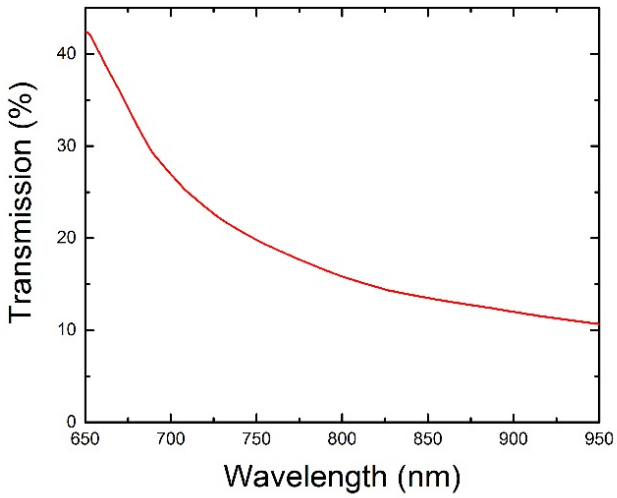

Figure 3.7 Au Transmission Spectrum at normal incidence angle

3.4 Results and Discussion

The red line in Figure 3.8 shows the FP filter transmission at the normal incident angle. There are three transmission peaks between 800 nm and 900 nm. The free spectral range in wavelength between 818.3 nm and 852 nm is 33.7 nm while the free spectral range in wavelength between 852 nm and 887.2 nm is 35.2 nm. The FSR increases with higher central wavelength as $\Delta\lambda_{FSR}$ rely on the λ^2 in the equation (3.15). The blue line in Figure 3.8 shows the laser spectrum with FP cavity filter at the normal incident angle. The lasing central wavelength is 852 nm and only one transmission peak shows in the SOA's spectral range, which is between 830 nm and 870 nm. The lasing peak matches the transmission peak of FP cavity filter at 852 nm in this figure.

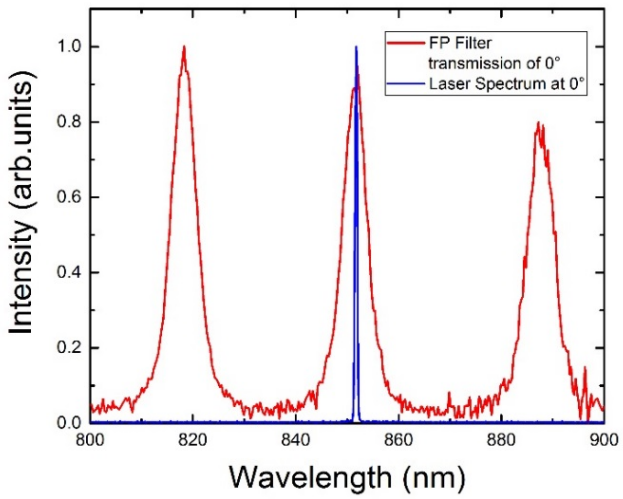

Figure 3.8 FP filter transmission and laser spectrum at normal incident angle

Figure 3.9 shows the output optical power versus injection current at the central wavelength of 856 nm. The blue dots represent the stimulated emission of the ECL with

FP filter and the red dots represent the spontaneous emission of SOA. The thresholds at each incident angle for the ECL with FP filter are different and the incident angle is controlled by stage controller. The threshold of this laser system reaches its lowest when tilts the incident angle of FP filter to 23°. The output power of this laser can as high as 3.5mW when the injection current reaches 70 mA. It is obvious that output optical power rapidly increases beyond threshold current but slowly increases below the threshold current. Below its threshold current, ECL with FP filter is dominated by the spontaneous emission.

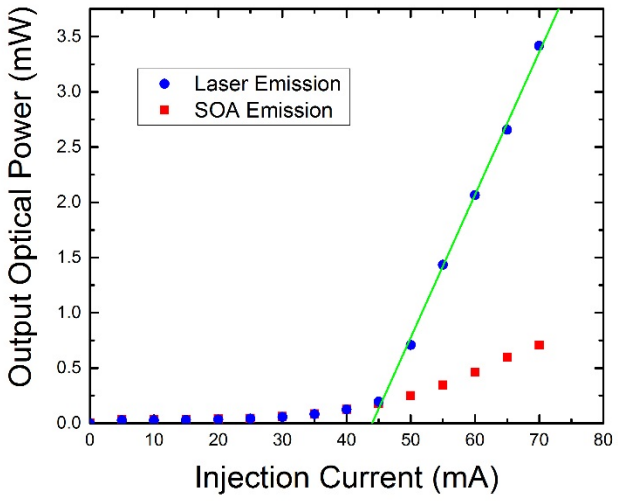

Figure 3.9 Power-current characteristics of external cavity laser with fiber collimator filter at central wavelength of 856 nm

When the threshold is higher than 44 mA, there is a distinct difference between laser emission (stimulated emission) and spontaneous emission that we can observe on Figure 3.9. The optical feedback in laser system results in the distinction between the

spontaneous emission and stimulated emission. The green straight that linear fitting stimulated emission shows the threshold of this laser.

The red line and blue line in Figure 3.10 show the FP filter transmissions with different incident angles. Transmission peak is located on 869 nm when the incident angle is 15.5°, whereas the transmission peak is shifted to 836 nm when the incident angle is 30°. 869 nm and 836 nm are the boundaries of our tunable ring laser. Therefore, the continuous tuning range for this system is 32 nm in the NIR region. As we can see in this figure, only one transmission peak shows in the spectral range of SOA, which is between 830 nm and 870 nm when tilts the incident angle.

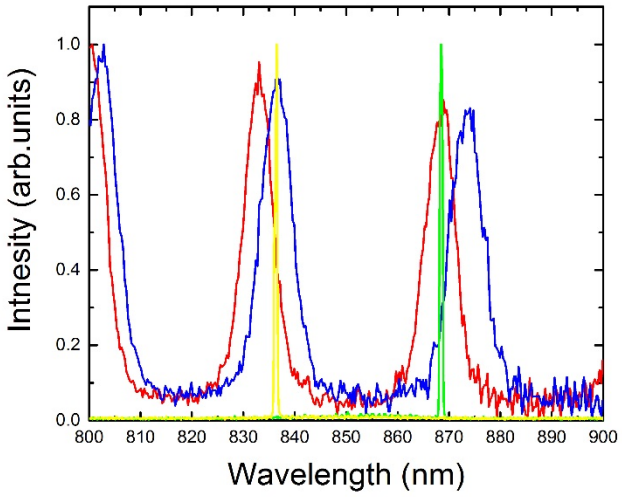

Figure 3.10 Fabry-Perot filter transmissions and laser spectrums with different incident angles (Red Line: Fabry-Perot filter transmission when tilts Fabry-Perot filter for 15.5°; Blue Line: Fabry-Perot filter transmission when tilts FP filter for 30.0°; Green Line: Tunable laser spectrum when tilts Fabry-Perot filter for 15.5°; Yellow Line: Tunable laser spectrum when tilts Fabry-Perot filter for 30.0°)

In Figure 3.10 the red peak which located at 869 nm moves lower as we increases the incident angle and reaches blue peak location at 836 nm. The consequence of increasing the incident angle is the reduction of central wavelength of transmission peaks. The reason that an increasing tilt angle decreases the wavelengths of the transmission peaks can be explained by equation (3.11). A plausible but wrong argument is that tilting broadens the gap (d) between two gold plates and it results in the increase of wavelength. However, phase shift to shorter wavelengths as we can explain in equation (3.7).

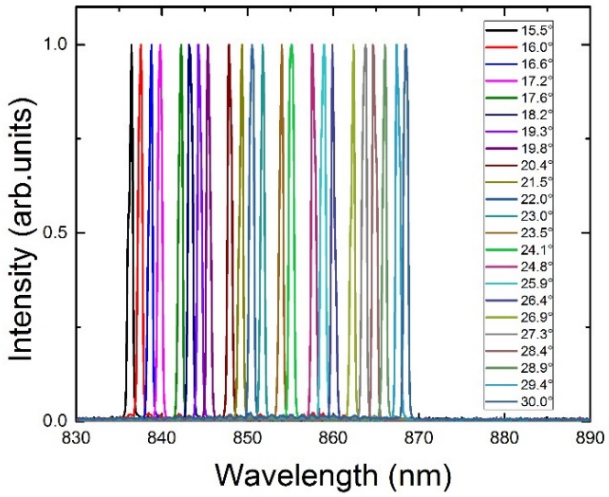

Figure 3.11 External cavity lasing spectrum with different Fabry-Perot filter angles

Figure 3.11 shows the different laser peaks of external cavity laser, when tilts the FP cavity filter. As shown in this figure, there are 23 peaks available for tuning between 832 nm and 868 nm. The range of tilting angles is 14. 5° which between 15.5° to 30°. In order to achieve wider laser tuning range, the start angle should start from 15.5°.

If the start angle is the normal incident angle ,the range from 852 nm to 868 nm is not including in the tuning range, because transmission peaks always move to lower wavelength. This phenomenon is easily to be explained by equation (3.11). The central wavelength of 852 nm which shown in Figure 3.8 has to decrease rather than increase as we explained before.

We just tilted the FP cavity filter by the stage controller and each angle gave a specific central wavelength. Therefore, we can tune this ECL continuously and smoothly. The signals showing on screen are stable and sharp.

Table 3.1 Corresponding ECL lasing wavelengths with each incident angle

Wavelength (nm)	Angle (degree)	Wavelength (nm)	Angle (degree)
868.46	15.5	850.53	23.5
867.42	16.0	849.37	24.1
866.03	16.6	847.85	24.8
864.63	17.2	845.33	25.9
863.76	17.6	844.26	26.4
862.36	18.2	843.17	26.9
859.91	19.3	842.27	27.3
858.94	19.8	839.83	28.4
857.53	20.4	838.83	28.9
855.15	21.5	837.56	29.4
854.00	22.0	836.47	30.0
851.77	23.0		

Table 3.1 shows the corresponding ECL lasing wavelengths with each incident angle of FP filter. The tunable spectral range is between 832 nm and 868 nm. When we

operate stage controller, the stage that holds the FP cavity filter starts to rotate to corresponding angle and the wavelength is selected by the filter.

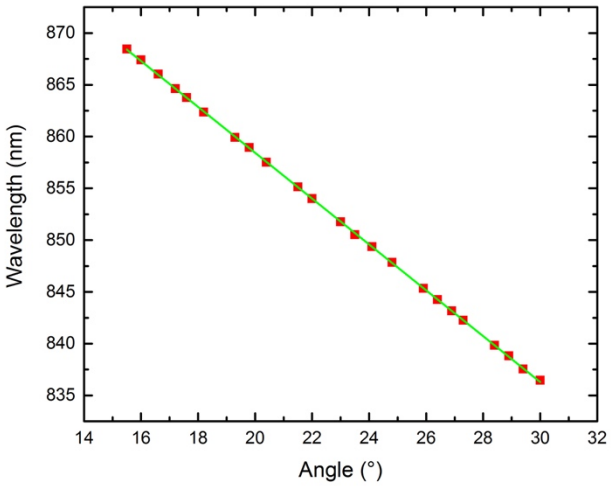

Figure 3.12 Selected wavelength varies with incident angle

Based on the collected data, there is a relationship between selected wavelength and incident angle as shown in Figure 3.12

$$Y=902.73-2.21*X \tag{2.2}$$

Where X is the incident angle and Y is selected wavelength. In conclusion, each fixed angle corresponds to a fixed selected lasing wavelength for the ECL with FP cavity filter.

3.5 Summary for Tunable Laser with Fabry-Perot Filter

A tunable external cavity laser utilizing a Fabry-Perot cavity filter and a semiconductor optical amplifier was proposed and demonstrated. The output wavelength

of the ECL is determined by the incident angle that is controlled by the stage controller. As the wavelength selective element for this ECL system, Fabry-Perot filter tunes the lasing range from 832 nm to 868 nm and more than 23 peaks can be found in this laser system.

CHAPTER 4. CONCLUSIONS

Tunable external cavity lasers with wide wavelength tuning width in near-infrared region were realized in this study. Some inexpensive components, such as SOA and fiber collimators, were used and two different wavelength selective filters were applied in two different laser systems. Tunable external cavity ring lasers in this thesis were comprised of two different wavelength selective elements. Different methods shown different effects for tuning range and accuracy. In the near-infrared region, wavelength tuning widths exceeded 27 nm in laser system with AOTF and 32 nm in laser system with FP filter. In the tunable external cavity ring laser system with acousto-optic tunable filter, the lasing central wavelength is decided by the input electrical RF frequency. However, the output wavelength in the tunable external cavity ring laser system with Fabry-Perot cavity filter is determined by the incident angle that is controlled by the stage controller. Laser threshold of 52 mA in system with AOTF and 44 mA in system with FP filter were obtained. Future aims are to reduce the optical coupling losses by optimizing the alignment technology related to the SOA-SOA direct coupling, optimize the wavelength selective filter for a high contrast, reduce the attenuations of each components in system, and improve the laser power.

REFERENCE

[1] SchäFer, F. P., And K. H. Drexhage. Dye Lasers. Berlin: Springer-Verlag, 1973.

[2] Duarte, F. J., And Lloyd William Hillman. Dye Laser Principles. Boston: Academic Press, 1990.

[3] T. W. Hänsch, Repetitively Pulsed Tunable Dye Laser for High Resolution Spectroscopy, Appl. Opt., 1972.

[4] Guenter Huber, Christian Kränkel, And Klaus Petermann., "Solid-State Lasers: Status and Future", 2010 Optical Society Of America, University Of Hamburg, Luruper Chaussee 149, D-22761 Hamburg, Germany, 2010.

[5] J. W. Crow and J. R. M. Craig, "Gaas Laser Linewidth Measurements By Heterodyne Detection" Appl. Phys. Lett., 1964.

[6] Bahaa E. A. Saleh, Malvin Carl Teich., "Fundamentals of Photonics" Wiley-Interscience, 2007.

[7] M. J. Connolly, Semiconductor Optical Amplifiers. Boston, Ma: Springer-Verlag, 2002.

[8] S.O.Kasap, "Optoelectronics And Photonics: Principles And Practices", University Of Saskatchewan, Canada, 2013.

[9] Niloy K. Dutta & Qiang Wang, "Semiconductor Optical Amplifiers", University of Connecticut, USA, 2013.

[10] M. Haridim, B.I. Lembrikov, Y. Ben-Ezra., "Semiconductor Optical Amplifiers", Holon Institute of Technology (Hit),52 Golomb Str., Holon 58102, Israel, 2011.

[11] Brimrose, "Acousto-Optic Tunable Filters Spectrally Modulate Light", Brimrose Corporation of America, USA, 2015.

[12] Brillouin, L. "Diffusion of Light and X-Rays by A Transparent Homogeneous Body". Annales De Physique, 1922.

[13] Debye, P.; Sears, F.W. "On The Scattering of Light by Supersonic Waves", 1932.

[14] Lucas, R.; Biquard, P. "Optical Properties of Solid and Liquid Medias Subjected to High-Frequency Elastic Vibrations". Journal De Physique, 1932.

[15] “Free Space Acousto-Optic Tunable Filter Aotf - Brimrose.” Accessed May 15, 2016. Http://Www.Brimrose.Com/Pdfandwordfiles/Aotf.Pdf.

[16] “Io-F-850 Fiber Isolator User Guide - Thorlabs.” Accessed October 28, 2014. Https://Www.Thorlabs.Com/Thorcat/17100/Io-F-850-Manual.Pdf.

[17] Zhu, Yingying; Zhang, Chunmin; Zhao, Baochang, “Design and Analysis of A Novel Non-Collinear Acousto-Optic Tunable Filter”, Optics Communications, 2012.

[18] Pavneet Kaur, Sukhmeen Kaur. “Acousto Optic Tunable Filters”. Dept. of Electronics and Communication Technology, Guru Nanak Dev Univ., Amritsar, Punjab, India, 3, July - Sept 2015.

[19] Fabry C. And Perot A., "Sur Les Franges Des Lames Minces Argentees Et Leur Application A La Mesure De Petites Epaisseur D’air,” Annales De Chimie Et De Physique, Vol. 12, 1897.

[20] Valis T., Hogg D., And Measures R., “Fibre Optic Fabry-Perot Strain Gauge”, Ieee Photonic Technology Letters, Vol. 2, No. 3, March 1990.

[21] Van Brakel A., “Blood Pressure Manometer Using A Bragg Gratin-Based Fabry-Perot Interferometer”, B.Ing Mini Dissertation, Rand Afrikaans University, Johannesburg (Sa), 2002.

APPENDIX. NOMENCLATURE

NIR	Near-Infrared
ECL	External Cavity Laser
SOA	Semiconductor Optical Amplifier
AOTF	Acousto-Optic Tunable Filter
FP	Fabry-Perot
ACC	Automatic Current Control
APC	Automatic Power Control
FC	Fiber Collimators
FSR	Free Spectral Range
FWHM	Full Width at Half Maximum
R	Reflectance
F	Finesse
λ	Wavelength
d	Thickness
θ	Incident Angle
n	Refractive Index
ASE	Amplifier Spontaneous Emission
TW	Traveling Wave
AR	Anti-reflection